HHS Public Access

Author manuscript

Kidney Int. Author manuscript; available in PMC 2016 January 01.

Published in final edited form as:

Kidney Int. 2015 July ; 88(1): 186–192. doi:10.1038/ki.2015.3.

Lipid imaging within the normal rat kidney using silver nanoparticles by matrix-assisted laser desorption/ionization mass spectrometry

Ludovic Muller[1,2,&], **Ajay Kailas**[1,&], **Shelley N. Jackson**[1], **Aurelie Roux**[1], **Damon Barbacci**[1,3], **J. Albert Schultz**[3], **Carey Balaban**[2], and **Amina S. Woods**[1,*]

[1]Structural Biology Unit, NIDA IRP, NIH, Baltimore, MD

[2]University of Pittsburgh, Pittsburgh, PA

[3]Ionwerks Inc., Houston TX

Abstract

The well-characterized cellular and structural components of the kidney show distinct regional compositions and distribution of lipids. In order to more fully analyze the renal lipidome we developed a matrix-assisted laser desorption/ionization mass spectrometry approach for imaging that may be used to pinpoint sites of changes from normal in pathological conditions. This was accomplished by implanting sagittal cryostat rat kidney sections with a stable, quantifiable and reproducible uniform layer of silver using a magnetron sputtering source to form silver nanoparticles. Thirty-eight lipid species including 7 ceramides, 8 diacylglycerols, 22 triacylglycerols, and cholesterol were detected and imaged in positive ion mode. Thirty-six lipid species consisting of, 7 sphingomyelins, 10 phosphatidylethanolamines, 1 phosphatidylglycerol, 7 phosphatidylinositols and 11 sulfatides, were imaged in negative ion mode for a total of seventy-four high resolution lipidome maps of the normal kidney. Thus, our approach is a powerful tool not only for studying structural changes in animal models of disease, but also for diagnosing and tracking stages of disease in human kidney tissue biopsies.

Keywords

MALDI mass spectrometric imaging (MALDI-MSI); kidney lipids; ceramides; silver nanoparticle matrix; tissue implantation; mass spectrometry

[*]**Corresponding Author:** Amina S. Woods, Ph.D., NIDA IRP, NIH, 333 Cassell Drive, Room 1120, Baltimore, MD 21224, Tel: 443-740-2747, Fax: 443-740-2144, awoods@mail.nih.gov.

[&]Co- first authors

Disclosure

All the authors declared no competing interests.

Introduction

The development of matrix-assisted laser desorption/ionization mass spectrometry (MALDI-MS) in the mid 1980's allowed for the surface analysis and detection of intact large biomolecules (proteins, peptides, lipids, etc.). (1,2) One of the major applications of MALDI-MS in the biological sciences has been the *in situ* analysis of molecules from tissue. This application was first demonstrated by Caprioli (3) but has since grown into the current technique of mass spectrometry imaging (MSI) that allows for high spatial resolution images that map individual molecules in tissue sections. (4–6) Although initial research using MSI focused on proteins and peptides, the use of MSI for the analysis of lipids in tissue has increased exponentially in recent years. (7–12) The key step in a MALDI MSI experiment is the addition of the matrix to the tissue section. The ideal method would produce a dry, uniform layer of matrix in order to preserve the integrity of the distribution of the molecules in the tissue. Recently, we have developed a method to implant silver nanoparticles (AgNPs) in tissue sections. (13) The stable, reproducible, and homogenous AgNPs matrix layer yielded high quality images of the regional distribution of several lipid classes. Since MSI is an *in situ* technique and thus does not allow for chromatographic separation, the selection of an appropriate matrix for the analytes of interest is vital for a successful MALDI experiment. Nanoparticle matrices have been more successful analyzing neutral lipids, such as cerebrosides, from tissue when compared to traditional solid (crystalline) matrices. (7,14,15) In particular, AgNPs have been used to image fatty acids in retinas (16) and triacylglycerols (TAGs) in heart tissue (13).

Although most work using MALDI for *in situ* analysis has focused on the brain, a several studies have applied this technique to the kidney. (17–21) These studies have included the profiling and imaging of lipids (17,18), proteins (19,20), and the cancer drug dasatinib (21). The kidneys are important to study as they play essential roles in the body's physiology such as maintaining homeostasis, regulating electrolyte balance, secreting the hormone renin that helps control blood pressure, serving as a blood filter, and removing waste such as urea and creatinine. With renal disease on the rise, MALDI-MSI is a powerful tool to investigate the renal pathology in animal models of kidney diseases. (22–24) Since applications of MALDI-MSI for disease models is rapidly expanding, it is vital to have a highly accurate and reproducible technique to generate images of the kidneys. Furthemore, it is of great interest for the researcher to have the opportunity to analyze different classes of biomolecules through the use of different MALDI matrices. This study mapped lipids in rat kidney by MALDI-MSI using AgNPs as a matrix with a MALDI-LTQ-Orbitrap (a high resolution mass spectrometer). Particular focus on neutral lipid classes such as TAGs, DAGs, and ceramides are highlighted.

Results and Discussion

Rat Kidney Structure

Figure 1 shows a light microscope picture of the kidney tissue section/ bregma used in this study. The mammalian kidney is divided into cortex, medulla, pelvis, and hilum. The cortex is often described as a cortical labyrinth full of renal corpuscles and adjacent tubules, while the medulla is less complex and contains the loop of Henle portion of the nephrons as well

as various vessels. The hilum is where the ureter and renal vessels are located. The pelvis, a minor region, contains the collecting ducts. The renal artery and vein, located in the hilum, branch off into the arcuate arteries and veins, which lie along the border between the cortex and medulla. The differential distribution of lipid species in the various anatomical regions of the rat kidney follows.

Analysis of Lipid Standards with AgNPs

Initial studies were conducted on standards from major lipid classes in the kidney. The standards were spotted directly on a kidney tissue section and then the section was implanted with AgNPs. The lipid standards were then analyzed in either/both positive and negative ion mode. The lipid standards tested were as follows: cholesterol$_{d7}$, Cer d18:1/12:0, SM d18:1/12:0, PC 14:0/14:0, PE 14:0/14:0, DAG 14:0/14:0, TAG 10:0/10:0/10:0, PG 18:1/18:1, PI 18:1/18:1, and ST d18:1/16:0. The mass spectrum obtained for each lipid is provided in the Supplemental Data section. Table 1 lists the major mass peaks observed for each lipid class. As has been observed previously(13), AgNPs in positive ion mode yield mass spectra that are dominated by the Ag adduct for neutral lipids (cholesterol, ceramide, DAGs, TAGs). The silver adducts offer two distinct advantages. First, Ag has two natural isotopes: ^{107}Ag (51.839%) and ^{109}Ag (48.161%). The twin silver isotope peaks are easily distinguished from other lipid mass peaks/background ions in the mass spectrum as long as there is sufficient mass resolution, approximately 50,000 for an m/z of 800. Secondly, silver is not naturally abundant in tissue as are Na and K. Thus, you can be ensured that the image of a Ag adduct lipid represents the natural (“true”) distribution, unlike a Na or K adduct, in which greater scrutiny has to be undertaken to be sure you are not imaging the distribution of Na/K. In positive mode, PE produced several major mass peaks (M-H+2K, M-H+ 2Na, M-H+NaK, and M-phosphoethanol head group+Ag) while PC only produced one dominant mass peak (M-phosphocholine head group+Ag). As noted in Table 1, caution has to be taken assigning PE and PC species based upon the fragment peak corresponding to the loss of their polar head group plus Ag. The reason is that these fragment peaks will have the same structure (DAG-H_2O+Ag) and thus the same m/z value if they have the same fatty acid backbone. Additionally, this same fragment peak can also be produced by DAGs and TAGs with the same fatty acid backbone. A similar pattern was also observed for SM in which the major peak was (M-phosphocholine head group+Ag) that is the same structure as ceramide-H_2O+Ag. Due to this, we only used silver adducts of intact lipid species to produce images in positive ion mode for this study.

In negative ion mode, AgNPs produced mass spectra that were very similar to those that are attained for lipids using more traditional organic matrices such as DHB. PE, PG, PI, and ST yielded mass spectra with one dominant mass peak (M-H), while SM also produced only one main mass peak (M-CH_2-H). Due to the simpler spectra, PE, PG, PI, ST, and SM were imaged in negative ion mode for the experiments below.

Distribution of Ceramides, Cholesterol, TAGs, and DAGs in Kidney in Positive Ion Mode

MALDI-MSI of kidney tissue sections using AgNPs in positive ion mode produce several high resolution ion images for Ag adducts of cholesterol, ceramides, DAGS and TAGS (Figure 2). A total of 38 lipid species (cholesterol, 7 Cers, 8 DAGs, 22 TAGs) were imaged

in the m/z range of 600–1100 Da. A list of all the lipid species imaged is provided in Supplemental Table 1 and images not shown in the text are provided in the supplemental data section. All the images and m/z calculations are based on the ^{107}Ag isotope except for the cholesterol+Ag_3 in which the most abundant isotope was used. However, for all the species imaged the corresponding ^{109}Ag adduct had the same distribution as the ^{107}Ag isotope.

Ceramides showed distinct and varying distribution based upon the fatty acid chain attached to the sphingosine backbone. Cer d18:1/22:0 at *m/z* 728.511 Da (Figure 2A) is highly localized in the medulla region of the kidney while CER d18:1/24:1 at *m/z* 754.526 Da (Figure 2B) is found in both the cortex and medulla with distribution across the cortical labyrinth and possible localization in the renal corpuscles and adjacent tubules of the nephron. Cer d18:1/26:0 at m/z 784.573 was detected only in the collecting tubules of the renal pelvis and was the only ceramide to show this distribution. The ability to detect intact ceramides is a major advantage for AgNPs compared to traditional organic matrices in which ceramides are usually detected as a fragment ion corresponding to a neutral loss of water $[Cer+H-H_2O]^+$.(25–27) This eliminates any confusion in assignment of ceramides compared to the water loss fragment peak that can arise from SMs and other sphingolipids.

Diacylglycerols (DAGS) are a class of neutral lipids with two fatty acids attached to a glycerol backbone. Most of the DAGs imagined in this study were localized mainly in the medulla. An example of this is DAG 34:1 (Figure 2E) which is concentrated in the medulla and also appears to be associated with the arcuate vessels at the cortico-medullary border. The localization of DAGs in the medulla is expected since the renal proximal tubular cells (located in the medulla) secrete Endothelin-1 which generates DAG. (28) DAG 32:0 at m/z 675.411 (Figure 2D) showed a more evenly distribution throughout the cortex. Cholesterol is one of the most abundant lipid species in mammalian cells. Although $[Cholesterol+Ag]^+$ was the major mass peak observed for cholesterol, we imaged the minor peak at 709.069 Da that corresponds to $[Cholesterol+Ag_3]^+$. This was done to limit the m/z range that we imaged in order to make the data file small enough to be opened and analyzed in our software. The peak at 709.069 Da represents the most abundant isotope and was distributed throughout the top of the kidney, but not in the hilum. All the isotopes of $[Cholesterol+Ag_3]^+$ showed the exact same distribution and these images are in the supplemental data section. In our previous work using DHB in positive ion mode, cholesterol was detected as a fragment ion $[cholesterol+H-H_2O]^+$. (29) However, AgNPs enabled the detection of intact cholesterol.

Triacylglycerols (TAGs) are a class of lipids comprised of glycerol and three fatty acids. Three main patterns of distribution for TAGs in the kidney were observed. Figure 2G illustrates the distribution of TAG 48:0 that is mainly distributed in the cortex. TAG 48:0 was the only TAG specie to show this distribution. The two more common patterns of distribution observed were cortex and hilum (Figure 2H, TAG 50:2) and mainly hilum (Figure 2I, TAG 54:5). In order to highlight the different regions of the kidney, Figure 3 contains a combo plot of DAG 38:4, Cer d18:1/24:0, and TAG 52:4. The combo plot shows the overlap of DAG 38:4 and Cer d18:1/24:0 in the cortex and medulla while TAG 52:4 is

concentrated in the hilum. The pelvis region of the kidney is highlighted by the presence of DAG 38:4.

Distribution of SMs, PEs, PGs, PIs, and STs in Kidney in Negative Ion Mode

Figure 4 highlights images obtained for a MALDI-MSI run of a kidney tissue section using AgNPs in negative ion mode. SMs were detected as $[M\text{-}CH2\text{-}H]^-$ mass peaks while all other lipid classes were imaged using the $[M\text{-}H]^-$ mass peak. A total of 36 lipid species (10 PEs, 1 PG, 7 PIs, 7 SMs, 11 STs) were imaged in the m/z range of 600–1100 Da. A list of all the lipid species imaged is provided in Supplemental Table 2 and images not shown in the text are provided in the supplemental data section. Sphingomyelin (SM) is a class of lipids consisting of a phosphocholine head group attached to a ceramide backbone. SMs displayed different distribution depending upon the fatty acid attached to the sphingosine base. SM d18:1/16:1 (Figure 4A) and SM d18:1/24:0 (Figure 4C) were mainly observed throughout the renal cortex. Figure 4B shows the distribution of SM d18:1/18:0, which is concentrated in the medulla region and within dot-like structures across the cortex, which are likely renal corpuscles of the nephron. Images from three classes of glycerolphospholipids (PEs, PGs, PIs) are illustrated in Figures 4D-I. The distribution appears to be more influenced by the fatty acid chains than the polar head groups. For example, PE 38a:4 (Figure 4E) and PI 38:4 (Figure 4H), both have the same fatty acid backbone, show similar distribution in which they are concentrated in the cortex region. Another finding illustrated in Figure 4I, is the localization of PI 32:0 in the cortex region almost exclusively. This is very similar to the distribution of DAG 32:0 (Figure 2D) and TAG 48:0 (Figure 2G) and suggest that lipids with only saturated fatty acids are concentrated in the cortex region.

Sulfatides are a class of sphingolipids with an additional sulfate group at the 3’ position of the galactose moiety in galactocerebroside. Additionally, sulfatides can be hydroxylated (OH) on their acyl chain. Figure 4J-L contains the ion map for 3 ST species as can be seen all the species are highly concentrated in the medulla. A previous study of mouse kidney found ST to be concentrated in the medulla. (18) Furthermore, sulfatides have been implicated in the transport of sodium chloride in the ascending loop of Henle (located in the medulla), which is in agreement with our findings in this study. (30) One additional result is that hydroxylation of the ST specie slightly changes its distribution. An example of this is ST d18:1/22:0 (Figure 4J) that is only observed in the medulla compared to ST d18:1/22:0 (OH) that is highly concentrated in the medulla but it is also observed in small channels that protrude out into the cortex. This result was observed for all hydroxylated ST species. Figure 5 contains a combo plot of SM d18:1/16:0, ST d18:1/24:1, and ST d18:1/24:1(OH). The various blending between the species forms multiple “rings” in the combo plot, corresponding to substructure layers in the kidney. Additionally, SM d18:1/16:0 is localized in the cortex with thin channels of ST d18:1/24:1(OH) snaking out into the cortex.

Conclusion

A total of seventy-four lipids were detected and imaged in the kidney using AgNPs, corresponding to cholesterol, 7 Cers, 8 DAGs, 22 TAGs for a total of thirty-eight images in positive ion mode and 10 PEs, 1 PG, 7 PIs, 7 SMs, 11 STs for a total of thirty-six images in

negative ion mode. AgNPs were proven to be a very effective matrix for the analysis of neutral lipids such as cholesterol, ceramides, DAGs, and TAGs in positive ion mode. For glycerophospholipids, the fatty acid chains influenced the distribution more than the different head groups for PEs, PGs, and PIs. Both DAGs and STs species were found to be heavily concentrated in the medulla region of the kidney. STs also sowed different distribution based upon whether the specie was hydroxylated or not. Another interesting finding was the concentration of lipid species containing only saturated fatty acids in the cortex. This was observed for several different lipid classes. Future MALDI-MSI studies should focus on tracking lipid changes as biomarkers for disease in afflicted and control rat models. Possible areas of study include, but are not limited to: diabetes, kidney stones, renal cancers, nephritis, and nephropathy.

Methods

Lipid Preparation

The following lipid standards: ceramide (Cer) d18:1/12:0, cholesterol d7, sulfatide (ST) d18:1/12:0, sphingomyelin (SM) d18:1/12:0, diacylglycerol (DAG) 14:0/14:0, phosphatidylcholine (PC)14:0/14:0, phosphatidylethanolamide (PE) 14:0a/14:0, phosphatidylglycerol (PG)14:0a/14:0, [purchased from Avanti Polar Lipids (Alabaster, AL)], and triacylglycerol (TAG) 10:0/10:0/10:0 [purchased from Sigma Aldrich (St. Louis, MO)], were prepared as stock solutions at 1–5mg/ml in CHL:MeOH (2:1 v/v). 0.5 uL of each solution were deposited directly on a kidney tissue section.

Tissue preparation

All the animal related work strictly adhered to the Guidelines for the Care and use of Laboratory Animals practiced at all institutes within the National Institutes of Health. The animals were male Sprague-Dawley rats (10–12 weeks old). After sacrifice, the rats were perfused with phosphate buffered saline and their organs immediately removed and frozen in dry ice chilled isopentane. Tissue sections were cut using a cryostat (Leica Microsystems CM3050S, Bannockburn, IL) at −21°C (cryochamber temperature) and -18°C (specimen cooling temperature). The kidney was attached to the cryostat specimen disk using ice slush made with distilled water (29), and 20 μm thick sections were obtained. The tissue sections were then placed on glass microscope slides for MALDI imaging.

NP Formation and Implantation

Kidney tissue sections were implanted with AgNPs using an NPlanter (Ionwerks, Houston, TX) which uses a magnetron sputtering source to form gas phase AgNP ions. AgNPs diameter range is 0.5–15nm. Silver targets are disks of 99.99% pure silver, 5 cm diameter×0.31 cm thick, purchased from Kurt J. Lesker Company (Clairton, PA). Nanoparticles sizes were selected using a quadrupole mass filter with a Gaussian diameter. We set the distribution to 6nm (2.5 nm FWHM). The selected particle beam was then accelerated to 500 eV and electronically rastered to ensure uniform deposition. The result is a thick 2–4 monolayer silver coated tissue sample. The deposition/tissue section takes 18 minutes. The NPlanter reduces the inherent variability between operators as it is an automated deposition. Furthermore, it is highly reproducible and results in images in which

you can compare raw counts from different tissue sections without the need to normalize by TIC. An example of this for three serial tissue sections is included in the supplemental data section.

Mass Spectrometer

A MALDI LTQ-XL-Orbitrap (Thermo Fisher, San Jose, CA) was used for data acquisition. Thermo's Imagequest and Xcalibur software were used for MALDI-MSI data processing. Images were acquired in both positive and negative ion mode, within a mass range of 600–1100 Da, with 3 laser shots per pixel, at a laser fluency of 14uJ in positive ion mode and 16uJ in negative ion mode. The target plate stepping distance was set to 50 μm with mass resolution of 30,000 for negative ion mode and 60,000 for positive ion mode. Custom-built IDL based software developed by Ionwerks, Inc was employed to extract peak lists from the tissue.

Lipid Assignment

Lipids were assigned as follows: PC, PI, PG, DAG, and TAG species number equal the total length and number of double bonds of acyl chains, while ceramide, SM and ST species number corresponds to the length and number of double bonds of the acyl chain attached to the sphigosine base. PE species number equal the total length and number of both radyl chains with **a** representing 1,2 diacyl species and **p** representing a 1-O-(1'-alkenyl)-2-acyl (plasmalogen) species. Lipids were assigned based upon a database search with a mass error less than 5 ppm. Tandem MS was also conducted to confirm assignments. Representative MS/MS data is provided in the supplemental data section.

Supplementary Material

Refer to Web version on PubMed Central for supplementary material.

Acknowledgements

This research was supported by the Intramural Research Program of the National Institute on Drug Abuse, NIH. The authors acknowledge Dr. Mari Prieto and Glen Gregory of the Thermo Fisher Corporation for technical and instrumentation advices. Ionwerks and the University of Pittsburgh gratefully acknowledge ARRA support through NIDA phase II SBIR grant 1RC3DA031431-01.

Abbreviations

SMs	sphingomyelins
CERs	ceramides
DAGs	diacylglycerols
PCs	phosphatidylcholines
TAGs	triacylglycerols
PEs	phosphatidylethanolamines
PG	phosphatidylglycerol

PIs	phosphatidylinositols
STs	sulfatides
HG	head group
AgNPs	silver nanoparticles
MALDI-MSI	MALDI-Mass Spectrometry Imaging

References

1. Tanaka K, Waki H, Ido Y, et al. Protein and Polymer Analyses up to *m/z* 100 000 by Laser Ionization Time-of-flight Mass Spectrometry. Rapid Commum Mass Spectrom. 1988; 2:151–153.
2. Karas M, Hillenkamp F. Laser Desorption Ionization of Proteins with Molecular Masses Exceeding 10 000 Daltons. Anal Chem. 1988; 60:2301–2303. [PubMed: 2977069]
3. Caprioli RM, Farmer TB, Gile J. Molecular Imaging of Biological Samples: Localization of Peptides and Proteins Using MALDI-TOF MS. Anal Chem. 1997; 69:4751–4760. [PubMed: 9406525]
4. Cornett DS, Reyzer ML, Chaurand P, Caprioli RM. MALDI imaging mass spectrometry: molecular snapshots of biochemical systems. Nat Methods. 2007; 4:828–833. [PubMed: 17901873]
5. Amstalden van Hove ER, Smith DF, Heeren RMA. A concise review of mass spectrometry imaging. J Chromatogr A. 2010; 1217:3946–3954. [PubMed: 20223463]
6. Seeley EH, Schwamborn K, Caprioli RM. Imaging of Intact Tissue Sections: Moving beyond the Microscope. J Biol Chem. 2013; 286:25459–25466. [PubMed: 21632549]
7. Jackson SN, Ugarov M, Egan T, et al. MALDI-ion mobility-TOFMS imaging of lipids in rat brain tissue. J Mass Spectrom. 2007; 42:1093–1098. [PubMed: 17621389]
8. Colsch B, Jackson SN, Dutta S, Woods AS. Molecular Microscopy of Brain Gangliosides: Illustrating their Distribution in Hippocampal Cell Layers. ACS Chemical Neuroscience. 2011; 2:213–222. [PubMed: 21961052]
9. Delvolve AM, Colsch B, Woods AS. Highlighting anatomical sub-structures in rat brain tissue using lipid imaging. Analytical Methods. 2011; 3:1729–1736. [PubMed: 21961026]
10. Fernández JA, Ochoa B, Fresnedo O, et al. Matrix-assisted laser desorption ionization imaging mass spectrometry in lipidomics. Anal Bioanal Chem. 2011; 401:29–51. [PubMed: 21308368]
11. Goto-Inoue N, Hayasaka T, Zaima N, Setou M. Imaging mass spectrometry for lipidomics. Biochimica et Biophysica Acta. 2011; 1811:961–969. [PubMed: 21440085]
12. Gode D, Volmer DA. Lipid imaging by mass spectrometry-a review. Analyst. 2013; 138:1289–1315. [PubMed: 23314100]
13. Jackson S, Baldwin K, Muller L, et al. Imaging of Lipids in Rat Heart with Silver Nanoparticles. Anal Bioanal Chem. 2014; 406:1377–1386. [PubMed: 24309627]
14. Cha S, Yeung ES. Colloidal Graphite-Assisted Laser Desorption/Ionization Mass Spectrometry and MSn of Small Molecules. Anal Chem. 2007; 79:2373–2385. [PubMed: 17288467]
15. Taira S, Sugiura Y, Moritake S, et al. Nanoparticle-Assisted Laser Desorption/Ionization Based Mass Imaging with Cellular Resolution. Anal Chem. 2008; 80:4761–4766. [PubMed: 18476721]
16. Hayasaka T, Goto-Inoue N, Zaima N, et al. Imaging Mass Spectrometry with Silver Nanoparticles Reveals the Distribution of Fatty Acids in Mouse Retinal Sections. J Am Soc Mass Spectrom. 2010; 21:1446–1454. [PubMed: 20471280]
17. Woods AS, Wang H-YJ, Jackson SN. A Snapshot of Tissue Glycerolipids. Curr Pharm Des. 2007; 13:3344–3356. [PubMed: 18045188]
18. Marsching C, Eckhardt M, Grone HJ, et al. Imaging of complex sulfatides SM3 and SB1a in mouse kidney using MALDI-TOF/TOF mass spectrometry. Anal. Bioanal. Chem. 2011; 401:53–64. [PubMed: 21359825]

19. Trede D, Schiffler S, Becker M, et al. Exploring Three-Dimensional Matrix-Assisted Laser Desoprtion/Ionization Imaging Mass Spectrometry Data: Three-Dimensional Spatial Segmentation of Mouse Kidney. Anal Chem. 2012; 84:6079–6087. [PubMed: 22720760]
20. Angel PM, Caprioli RM. Matrix-Assisted Laser Desorption Ionization Imaging Mass Spectrometry: In Situ Molecular Mapping. Biochemistry. 2013; 52:3818–3828. [PubMed: 23259809]
21. Schulz S, Gerhardt D, Meyer B, Seegel M, et al. DMSO-enhanced MALDI MS imaging with normalization against a deuterated standard for relative quantification of dasatinib in serial mouse pharmacology studies. Anal Bioanal Chem. 2013; 405:9467–9476. [PubMed: 24121470]
22. Kaneko Y, Obata Y, Kakeya H, et al. Imaging mass spectrometry analysis reveals an altered lipid distribution pattern in the tubular areas of hyper-IgA murine kidneys . Exp Mol Pathol. 2011; 91:614–621. [PubMed: 21798258]
23. Lalowski M, Magni F, Mainini V, et al. Imaging mass spectrometry: a new tool for kidney disease investigations. Nephrol. Dial. Transplant. 2013; 7:1648–1655. [PubMed: 23553250]
24. Ruh H, Salonikios T, Fuchser J, et al. MALDI imaging MS reveals candidate lipid markers of polycystic kidney disease. J Lipid Res. 2013; 54:2785–2794. [PubMed: 23852700]
25. Hankin JA, Farias SE, Barkley RM, et al. MALDI mass spectrometric imaging of lipids in rat brain injury models. J Am Soc Mass Spectrom. 2011; 6:1014–1021. [PubMed: 21953042]
26. Goto-Inoue N, Hayasaka T, Zaima N, et al. Imaging Mass Spectrometry Visualizes Ceramides and the Pathogenesis of Dorfman-Chanarin Syndrome Due to Ceramide Metabolic Abnormality in the Skin. Plos One. 2012; 7:e49510. [PubMed: 23145181]
27. Wang H-YJ, Wu HW, Tsai PJ, Liu CB. MALDI-mass spectrometry imaging of desalted rat brain sections reveals ischemia-mediated changes of lipids. Anal Bioanal Chem. 2012; 1:113–124. [PubMed: 22610601]
28. Beara-Lasic L, Knotek M, Cejvan K, et al. The effect of big endothelin-1 in the proximal tubule of the rat kidney. Br J of Pharmacol. 1997; 120:625–630. [PubMed: 9051300]
29. Jackson SN, Wang H-YJ, Woods AS. Direct Profiling of Lipid Distribution in Brain Tissue Using MALDI-TOFMS. Anal Chem. 2005; 77:4523–4527. [PubMed: 16013869]
30. Zalc B, Helwig JJ, Ghandour MS, Sarlieve L. Sulfatide in the kidney: how is this lipid involved in sodium chloride transport? FEBS Letters. 1978; 92:92–96. [PubMed: 149676]

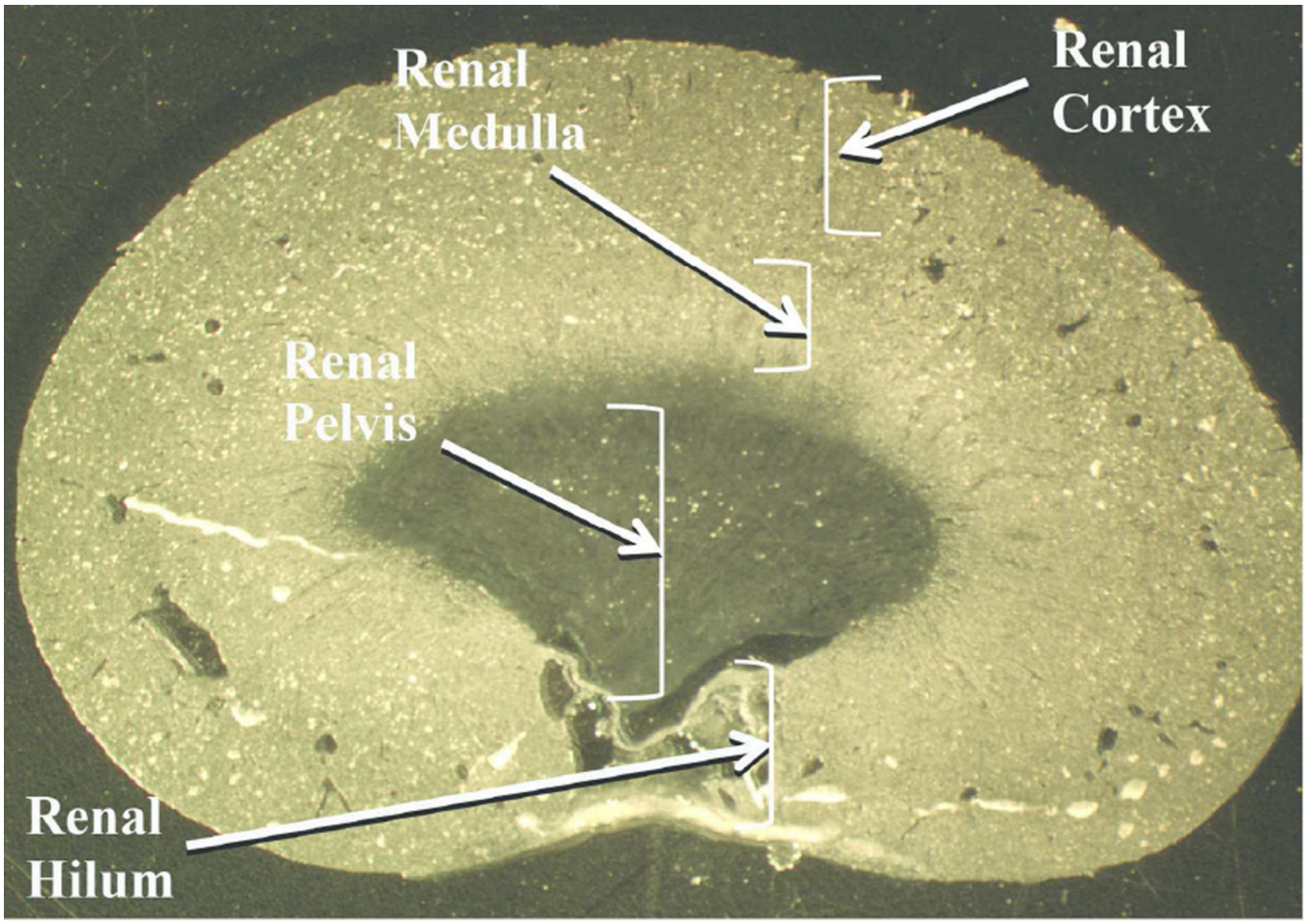

Figure 1.
Light microscope picture of kidney section/ bregma used for MALDI imaging in this study.

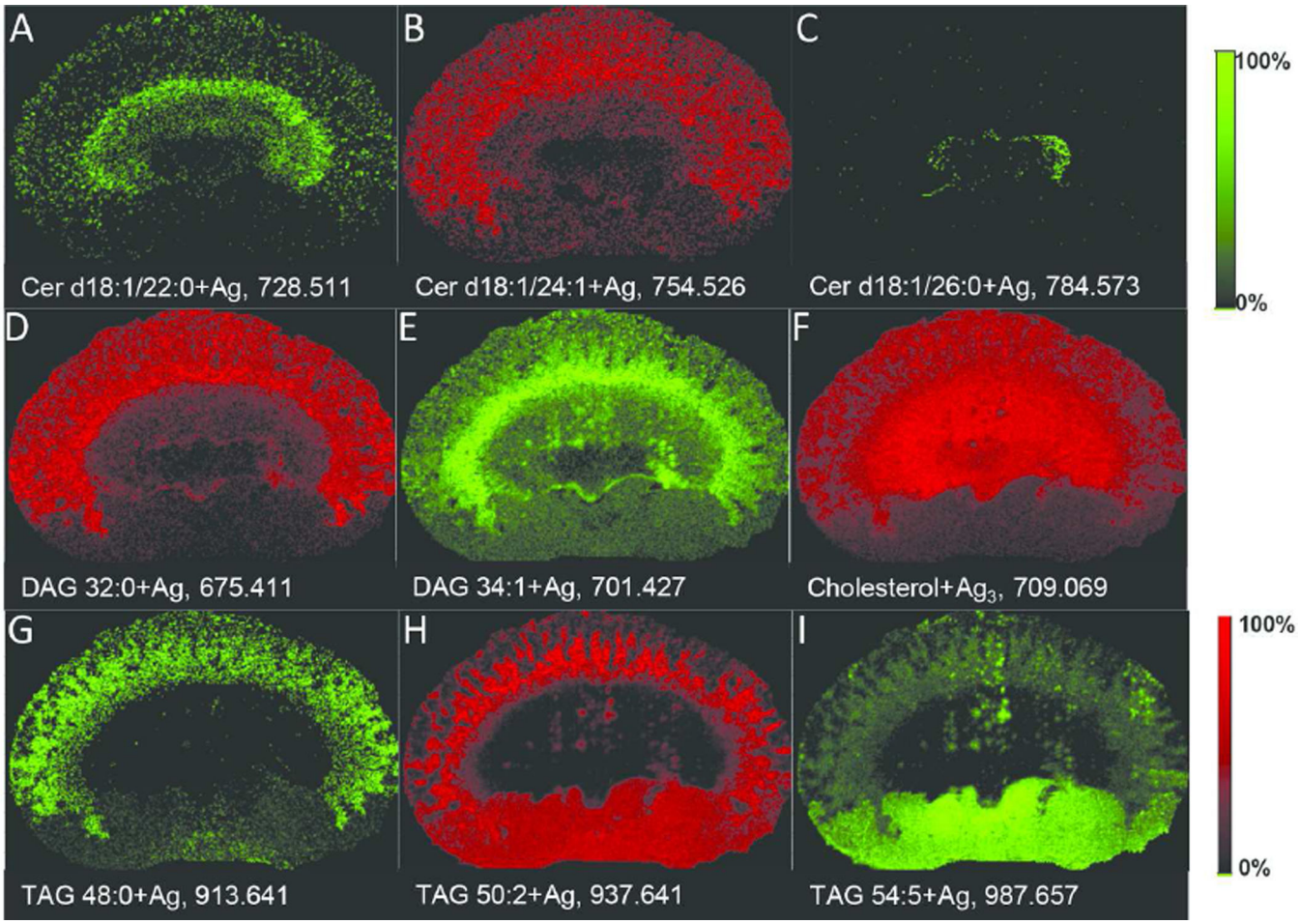

Figure 2.

MALDI images of (A) Cer d18:1/22:0+Ag, 728.511 Da (B) Cer d18:1/24:1+Ag, 754.526 Da (C) Cer d18:1/26:0+Ag, 784.573 Da (D) DAG 32:0+Ag, 675.411 Da, (E) DAG 34:1+Ag, 701.427 Da (F) Cholesterol+Ag_3,709.069 Da (G) TAG 48:0+Ag, 913.641 Da (H) TAG 50:2+Ag, 937.641 Da (I) TAG 54:5+Ag, 987.657 in kidney tissue section with AgNPs in positive ion mode.

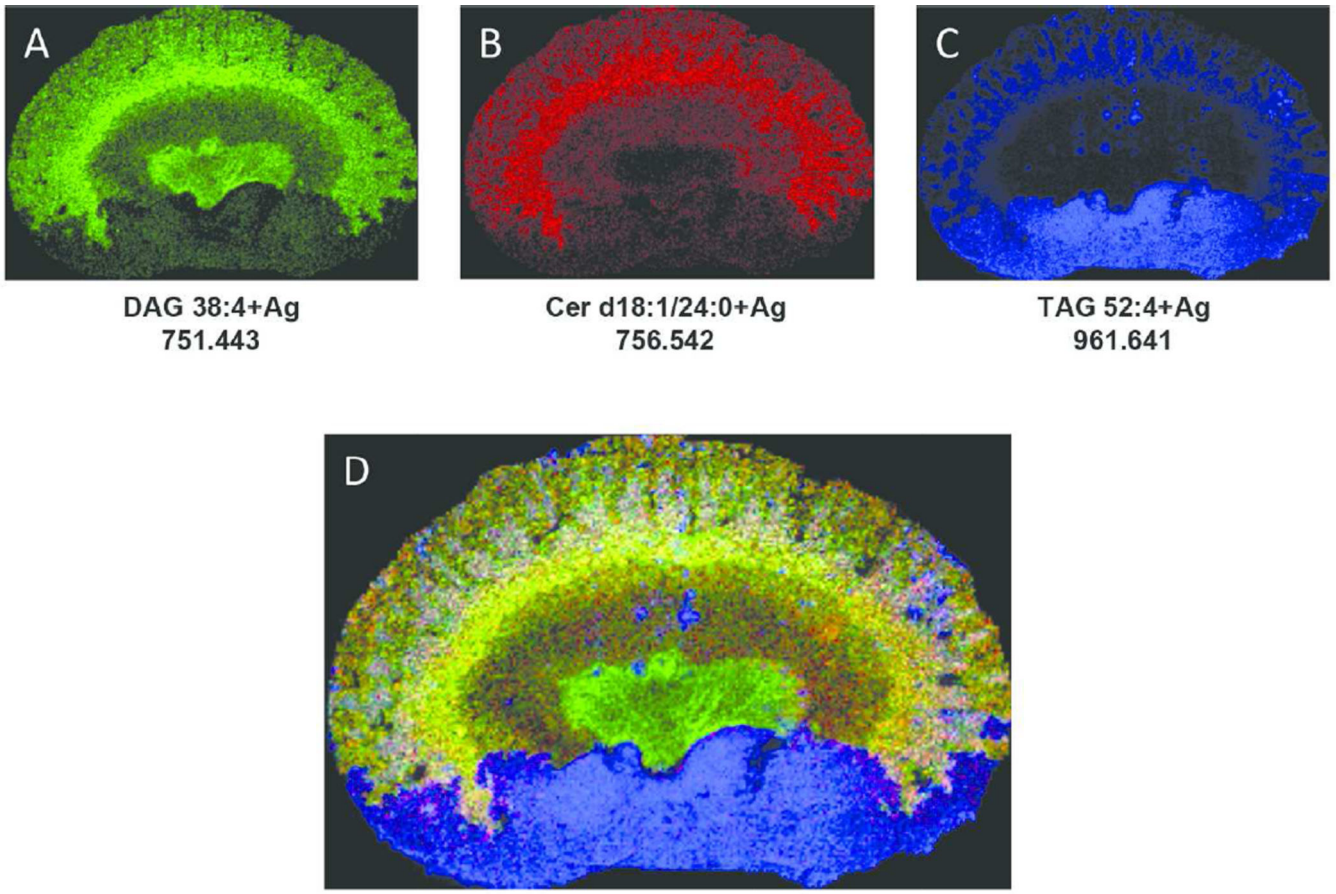

Figure 3.

MALDI images of kidney tissue implanted with AgNPs in positive ion mode showing the distribution of: (A) DAG 38:4+Ag, 751.443 Da (B) Cer d18:1/24:0+Ag, 756.542 Da (C) TAG 52:4+Ag, 961.641 (D) Triple Combination Plot of 751.443 (green), 756.542 (red), and 961.641 (blue).

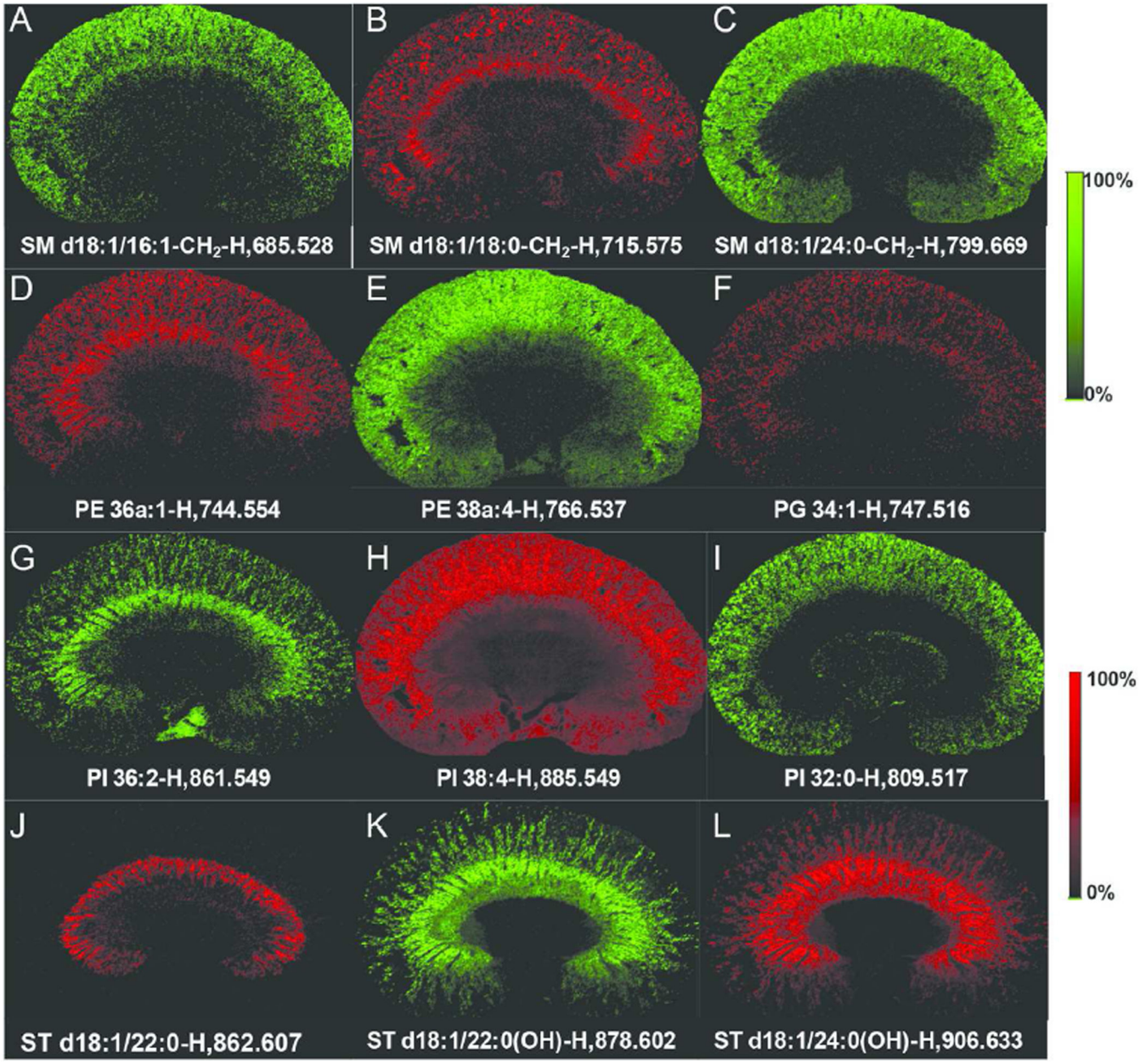

Figure 4.

MALDI images of (A) SM d18:1/16:1-CH_2-H, 685.528 Da (B) SM d18:1/18:0-CH_2-H, 715.575 Da (C) SM d18:1/24:0-CH_2-H, 799.669 Da (D) PE 36a:1-H, 744.554 Da, (E) PE 38a:4-H,766.537 Da (F) PG 34:1-H, 747.516 Da (G) PI 36:2-H, 861.549 Da (H) PI 38:4-H, 885.549 Da (I) PI 32:0-H, 809.517 Da (J) ST d18:1/22:0-H, 862.607 Da (K) ST d18:1/22:0(OH), 878.602 (L) ST d18:1/24:0(OH), 906.633 Da in kidney tissue section with AgNPs in negative ion mode.

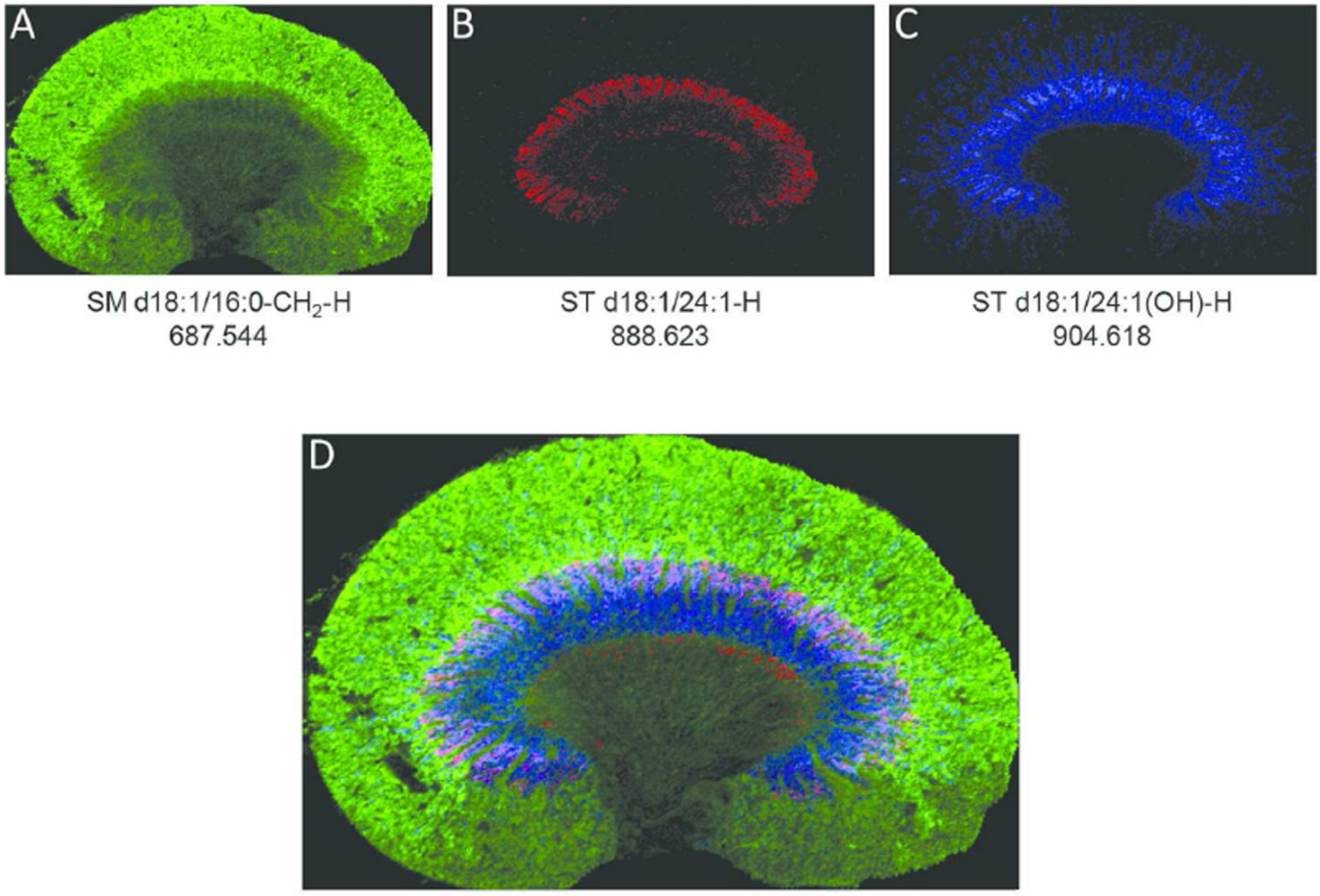

Figure 5.

MALDI images of kidney tissue implanted with AgNPs in negative ion mode showing the distribution of: (A) SM d18:1/16:0-CH2-H, 687.544 Da (B) ST d18:1/24:1-H, 888.623 Da (C) ST d18:1/24:1(OH), 904.618 Da (D) Triple Combination Plot of 687.544 (green), 888.623 (red), and 904.618 (blue).

Table 1

Mass peaks observed for Lipid Standards using AgNPs.

Lipid	Positive Ion Mode	Negative Ion Mode
Cholesterol	**M+Ag**, M-H+2Ag, M+Ag_3	---
Ceramide	**M+Ag, M-H_2O+Ag** (Cer-H_2O)	---
Sphingomyelin	M+Ag, M+K, M+Na, **M-HG+Ag** (Cer-H_2O)	**M-CH_2 -H**
Phosphatidylcholine	M+Ag, M+K, M+Na, **M-HG+Ag** (DAG-H_2O)	---
Phosphatidylethanolamine	M+Ag, M+K, M+Na, M-H+NaAg, M-H+KAg, **M-H+2K**, **M-H+2Na**, **M-H+NaK**, **M-HG+Ag** (DAG-H_2O)	**M-H**
Diacylglycerol	**M+Ag**, M+K, M+Na, M-H_2O+Ag (DAG-H_2O)	---
Triacylglycerol	**M+Ag**, **M-acyl group+Ag** (DAG-H_2O)	---
Phosphatidylglycerol	---	**M-H**
Phosphatidylinositol	---	**M-H**
Sulfatide	---	**M-H**

Bold represents major mass peaks. HG = polar head group for lipid class (Cer-H_2O) and (DAG-H_2O) indicates fragment peaks that will have the same structure and m/z value if lipid species have the same acyl groups (fatty acid chains).